

ARTICLES

Laplacian of the Electronic Charge Density and Heat of Adsorption of O₂ and CO Molecules on 3d Transition Metals

Yosslen Aray,* Jesus Rodriguez, and David Vega†

Centro de Quimica IVIC, Apartado 21827 Caracas 1020 A, Venezuela

Received: October 12, 1999; In Final Form: March 2, 2000

A topological analysis of the Laplacian of the electronic charge density of bulk 3d transition metals has been performed. This analysis shows that the atomic graph for the atoms of the fcc metals (Ni and Cu) is an octahedron with six vertexes (corresponding to local charge concentrations) linked by twelve edges and bounded by eight faces (corresponding to local charge minima). For the bcc case (V, Cr, and Fe), the corresponding graph is a cube with eight vertexes, twelve edges, and six faces. For the early hcp metals (Sc and Ti), the graph is a trigonal bipyramid with five vertexes, nine edges, and six faces, whereas for Co, it is a trigonal prism with six vertexes, nine edges, and five faces. Despite the different kinds of the graphs obtained, we have been able to correlate the value of the Laplacian at the local minima with the experimental heats of adsorption (which show a systematic decrease) for the O₂ and CO molecules on the 3d transition metals. This result suggests that the bonds formed by these molecules with 3d transition metals become stronger for cases in which the local charge minima of the metal atom decreases.

1. Introduction

The Laplacian of the charge density, $L(\mathbf{r}) = -\nabla^2\rho(\mathbf{r})$, is a very useful tool for extracting chemical information¹ contained in the charge density of molecular systems and materials, and, in addition, it is particularly important for the purpose of understanding chemical reactivity.^{1–5} The underlying reason is that it allows us to establish a correlation between the critical points, CPs, of $L(\mathbf{r})$ in the valence shell and the location of the active sites in molecules. In general, a Lewis acid–base reaction occurs due to the fact that a local charge concentration (a maximum on $L(\mathbf{r})$) of the valence shell on the base aligns itself with a local charge depletion (a minimum on $L(\mathbf{r})$) on the acid. This general phenomenon is observed in many different kinds of interactions,⁵ such as, for example, the formation of hydrogen bonds,⁶ the alignment of chlorine molecules in the solid state,⁷ and the adsorption of molecules on a surface.^{8–13} Through the study of the topology of the Laplacian,^{12,13} one is able to predict that the adsorption pathway of the CO molecule on the Fe, Ni, Cu, Rh, Pd, and Ag (100) surface, which is initially determined by the mutual alignment of a local maximum located on the C atom, C_v , with a local minimum on the top atoms of the surface, F_{top} . By means of this interpretation, one is also able to predict that the strength of the interactions increases with a decrease in $L(\mathbf{r})$ at F_{top} . Thus, this topological approach has the advantage of allowing us to directly interpret the reactivity of molecules on surfaces in terms of properties of $\rho(\mathbf{r})$ (an observable) without having to resort to nonobservable quantities, such as Mulliken

population indices, or to details of specific set of molecular orbitals.

One of the most important functions ascribed to transition metals (TM) in catalytic reactions is that of atomizing diatomic molecules, such as CO and O₂, and then of supplying the resulting atoms to other reactants and reaction intermediates.¹⁴ A very important parameter influencing the dissociation rate of molecules on TM is the adsorption energy. In general, two main parameters determine the rate of dissociation of the O₂ and CO molecules: the sticking probability and the adsorption energy.¹⁵ The latter should depend linearly on the degree of TM d-band filling: the heat of adsorption, ΔH_{ads} , which is a measure of the bond strength, steadily decreases from left to right¹⁵ along the first transition metal row in the Periodic Table. The adsorption energy of small molecules on TM crucially depends on the nature of the metal. In contrast, the surface crystallographic characteristics have a surprisingly small effect on ΔH_{ads} .^{16–17} Thus, differences in ΔH_{ads} are often larger between different materials than they are between different faces of the same material. As an example,¹⁶ let us mention that the heats of adsorption of CO on the (111) surface for Ni and Cu are 26.5 and 12.0 kcal/mol, respectively, whereas on the (100) surface they are 30.0 and 13.5 kcal/mol, respectively. Hence, important information may be obtained from the study of the correlation between the adsorption energy and the bulk properties of these materials. Along this vein, in the present work, we have determined the CPs of $L(\mathbf{r})$ in the valence shell of the bulk atoms of the 3d TM (Sc, Ti, V, Cr, Fe, Co, Ni, and Cu) and have explored their relationships with the experimental ΔH_{ads} of the O₂ and CO molecules on those catalysts. In addition, bearing in mind that catalysis is largely a surface event, we have also studied in details the CPs of the valence shell for

* To whom correspondence should be addressed. E-mail: yaray@quimica.ivic.ve. Fax: (58) 2 504 1350.

† Permanent address: FACYT. Universidad de Carabobo. Valencia, Venezuela. E-mail: dvega@thor.uc.edu.ve.

atoms in various surfaces of the same metals in order to compare them with bulk results.

2. Theory

The topological properties of a scalar field, such as $\nabla^2\rho$, are summarized by its critical points (CP).⁵ These are points in which the gradient vector field, $\nabla(\nabla^2\rho)$ vanishes, and they are classified according to their type (m,n) by stating their rank m and signature n . The rank is equal to the number of nonzero eigenvalues of the Hessian matrix of $\nabla^2\rho$, and the signature is given by the algebraic sum of the signs of the eigenvalues of $\nabla^2\rho$.

The Laplacian determines the regions of space in which the electronic charge is locally concentrated or depleted.^{1–3} Wherever $\nabla^2\rho$ is negative, there is a local concentration of charge, that is, the electronic density is greater than the average density in the immediate neighborhood. Wherever $\nabla^2\rho$ is positive, there is an analogous local depletion of charge. Because electron density is concentrated where $\nabla^2\rho < 0$, the topology of the Laplacian is conveniently given in terms of $L(\mathbf{r}) = -\nabla^2\rho$. In general, the atomic Laplacian⁵ exhibits alternating shells of charge concentration and charge depletion equal in number to the number of quantum shells. The outer valence shell of charge concentration (VSCC) contains a spherical surface over which ρ is maximally concentrated. The distribution of $L(\mathbf{r})$ over this surface is uniform for a free atom (if one assumes that the nucleus has a negligible electric quadrupole moment). Although this surface persists when the atom is in chemical combination, it no longer evinces a uniform concentration. The formation of a bond produces changes in this distribution, and a number of local maxima, minima, and saddle points appear on this surface of charge distribution.⁵ The localized concentrations of charge mimic the pairs of electrons assumed in the Lewis model in number, relative position, and sizes.

The radial curvature, that is, the curvature of $L(\mathbf{r})$ normal to the spherical surface contained in the VSCC, is negative. On the other hand, the two tangential curvatures can assume either positive or negative values. If both of these curvatures are negative or positive, then a local maximum (a (3,–3) CP) or a local minimum (a (3,+1) CP) is formed, respectively, on the surface. For cases in which one of the tangential curvatures is negative and the other positive, a saddle (a (3,–1) CP) is formed. Each maximum³ is linked to another by unique pairs of trajectories of the gradient of $L(\mathbf{r})$, which originate at the saddle points. The network of those trajectories partitions the surface of charge concentration into segments having curved faces. In the center of each one of these faces belonging to the VSCC surface is a local minimum. This structure is called an atomic graph^{3,4} (AG) and succinctly summarizes the types and the number of CPs formed on the surface of charge concentration of an atom in a molecule. This graph provides the connectivity of the extremes of $L(\mathbf{r})$ in the corresponding surface of charge concentration of the VSCC distribution. The AG is most easily visualized in terms of a polyhedron whose vertexes (V), edges (E), and faces (F) satisfy Euler's formula⁴

$$V - E + F = 2$$

The (3,–3) CPs (local maxima) define the vertexes. The unique pair of trajectories that originate at the (3,–1) CPs define the edges, and the (3,+1) CPs (local minima) define the faces. Making use of this graph, a Lewis acid–base reaction, customarily described in terms of aligning the charge concentration of the VSCC on the base with the charge depletion on the

TABLE 1: Values of $L(\mathbf{r})$ at the VSCC Critical Points of the 3d Transition Metal Atoms (atomic units)^a

		critical points		
		eight (3,–3)	twelve (3,–1)	six (3,+1)
bcc				
	V	13.562	12.683	10.125
	Cr	20.868	18.433	11.509
	Fe	32.428	31.204	27.554
		critical points		
		six (3,–3)	twelve (3,–1)	eight (3,+1)
fcc				
	Ni	59.561	49.651	46.404
	Cu	69.136	65.313	64.037
		critical points		
		five (3,–3)	nine (3,–1)	six (3,+1)
hcp ^b				
	Sc	one above 5.796 three in 5.931 one below 5.796	three above 5.777 three in 5.658 three below 5.777	5.651
	Ti	one above 9.398 three in 9.543 one below 9.398	three above 8.460 three in 8.307 three below 8.460	7.8930
		critical points		
		six (3,–3)	six (3,–1)	five (3,+1)
hcp ^b				
	Co	40.271	40.125	one above 39.152 three in 39.235 one below 39.152

^a 1 au of $L(\mathbf{r}) = 1 \text{ e}/a_0$.⁵ ^b When necessary, the position of the CPs are given with respect to the (0001) plane.

acid, may be alternatively described by directing a vertex of the graph for the base atom toward the face of the polyhedron for the acid.

3. Method

The electronic densities were calculated by means of the WIEN-97¹⁸ program using the Kohn–Sham Hamiltonian with the generalized gradient approximation of Perdew et al.¹⁹ and the unrestricted scheme to obtain spin-polarized wave functions. In view of the fact that WIEN-97 contains a full-potential linearized-augmented plane-wave (FLAPW) method,¹⁸ it may be considered as one of the very accurate methods currently available for performing electronic structure calculations in crystals. The unit cell is divided into nonoverlapping atomic spheres (centered at the atomic sites) and an interstitial region. In the two types of regions, different basis sets are used: a linear combination of radial functions times spherical harmonics inside the atomic sphere and a plane expansion in the interstitial region. Ninety-six points over the Brillouin Zone and quadratic tetrahedron method were chosen for k-space numerical integration. The topology of $L(\mathbf{r})$ was analyzed using a local version of the BUBBLE program²⁰ contained in NUMLAP²¹ and adapted for the WIEN 97 code.

4. Results and Discussion

The lattices of bulk transition metals²² considered in this work are described by the space group $Im\bar{3}m$ for body-centered cubic (bcc) structures (with parameters $a = 3.0282$, 2.8846 , and 2.8664 Å for V, Cr, and Fe, respectively) by the $Fm\bar{3}m$ space group for face-centered cubic (fcc) structures (with $a = 3.5236$ and 3.6147 Å for Ni and Cu, respectively) and by the $P6_3/mmc$ space group for hexagonal close-packed (hcp) structures (with $a =$

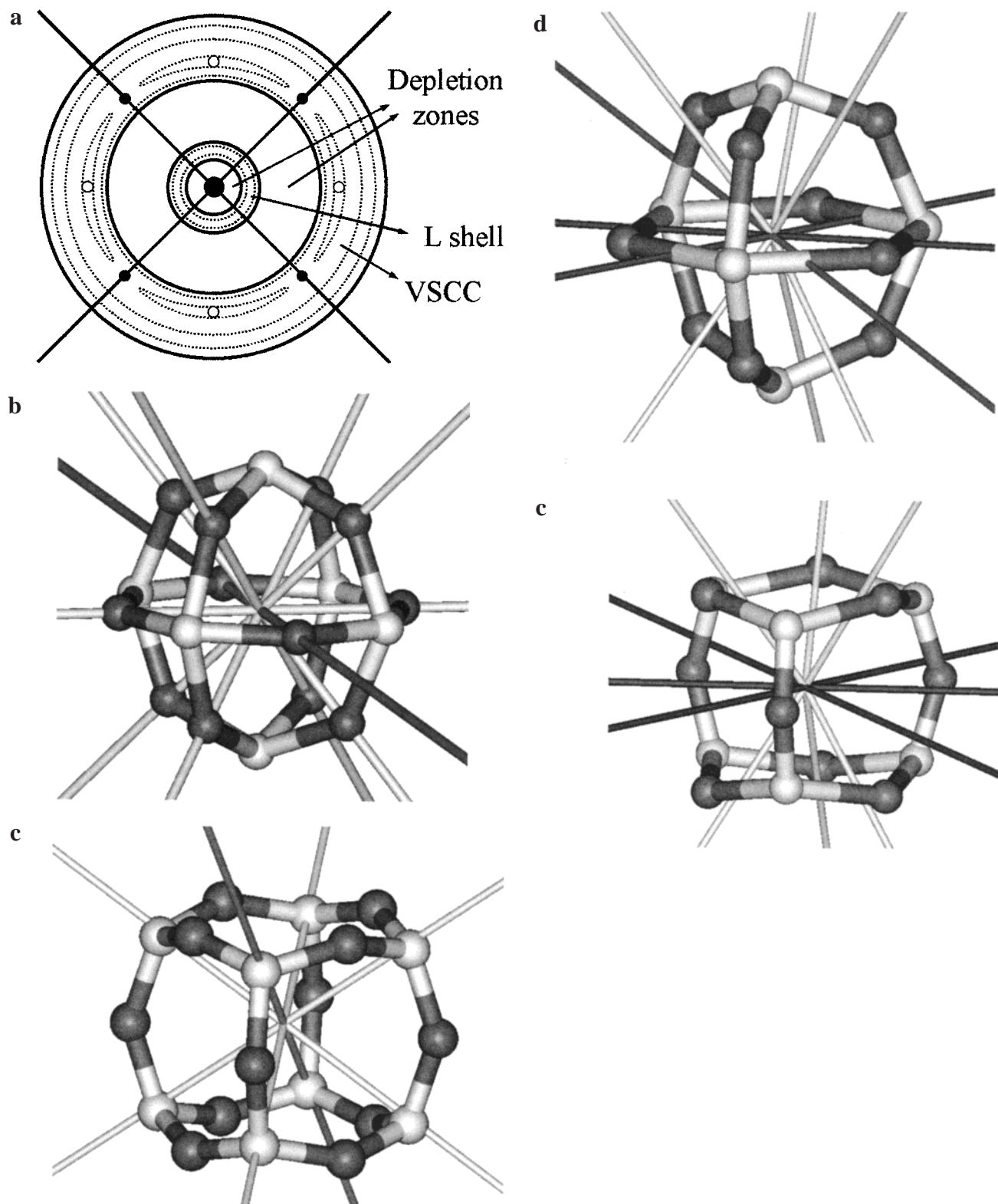


Figure 1. (a) Contour map of $L(r)$ of the Cu bulk atom on the (100) plane. The contour (dotted lines) values of the VSCC are -10.0, -30.0, and -65.0 au. The outermost contour is -10.0 au. The (3,-3) CPs are denoted by open dots, whereas the (3,-1) ones are denoted by full dots. The borders of the shells (solid rings) correspond to the 0.0 au contour's value. Bold straight lines point toward the first nearest neighbors. (b-e) Atomic graph for the bulk atom of the 3d transition metals: (b) fcc metals, (c) bcc metals, (d) Early hcp metals, and (e) hcp Co. White spheres denote the vertices (local charge concentrations or (3,-3) CPs) and gray spheres denote the edges (a (3,-1) CP). Long, straight lines indicate bonds with first nearest neighbors. In addition, in hcp graphs, black lines indicate the position of the second nearest neighbor.

2.9506, 2.506 and $c = 4.6788, 4.069$ Å for Ti and Co, respectively). To define the fcc and the bcc structures, it is only needed that an atom be placed at the origin of the cubic unit cell. Each atom in the bcc type has eight first nearest neighbors at a distance $a\sqrt{3}/2$ and another six second nearest neighbors

at a distance a , the cube's edge length. For fcc, which is a more closely packed structure, each atom has 12 eight first nearest neighbors placed at a distance $a\sqrt{2}/2$ and also has six second nearest neighbors at a distance a . To define the structure of the hcp metals, it is just necessary to locate an atom at the $1/3, 2/3$,

1/4 cell positions. In this case, each atom has six first nearest neighbors (three above and three below) placed at a distance $(a^2/3 + c^2/4)^{1/2}$ and six second nearest neighbors at a distance a .

We have located the critical points of $L(\mathbf{r})$ on the VSCC of the transition metal atoms considered in this work. The number, positions, and $L(\mathbf{r})$ values at the calculated CPs are displayed in Table 1, and Figure 1a illustrates the presence of the (3,-3) and (3,-1) CPs of the VSCC on the (100) plane of the bulk for Cu. The metallic atoms, as in the free atoms^{1d} and the carbonyl complexes,^{1b} $\text{Cr}(\text{CO})_6$, $\text{Fe}(\text{CO})_5$, and $\text{Ni}(\text{CO})_4$, only exhibited three shells of charge concentration. The VSCC is formed by the 3s3p3d (and 4s in the case of Cu) electrons. The VSCC of the atoms corresponding to fcc metals showed six local maxima and twelve (3,-1) CPs, pointing toward the second and the first nearest neighbors, respectively. Therefore, the atomic graph is an octahedron (Figure 1b) with six vertexes linked by twelve edges and eight local minima in the middle of the limiting faces. For the bcc case, the ensuing VSCC has eight local maxima or (3,-3) CPs pointing toward the eight first nearest neighbors and twelve (3,-1) CPs defining an atomic graph (Figure 1c) with eight vertexes linked by twelve edges and six faces joining these vertexes. From inspection of the band structure, we see that for V and Cr, the valence d-electrons occupy the t_{2g} bands (d_{xy} , d_{xz} , d_{yz}), whereas in the case of Fe, the e_g bands (d_{z^2} , $d_{x^2-y^2}$) are additionally occupied. Perfect electron pairing is observed in V and Cr, but in the case of Fe, there are 2.35 unpaired electrons. Let us note, however, that despite the difference in electronic structure, Fe has exactly the same atomic graph as the other bcc transition metals. The hcp metals exhibit different atomic graphs. The VSCC of the early TM atoms Sc and Ti (which have fewer d-electrons and are placed to the left of the bcc metals) have five local maxima, nine saddles (3,-1), and six local minima or (3,+1) CPs. The atomic graph is, in this case, a trigonal prism (Figure 1d) with six vertexes (three of which are located in the second nearest neighbors plane, whereas the other two point toward the first nearest neighbors) linked by nine edges and six faces. For Co, which is located to the right of the bcc metals and whose d-bands are almost filled, the VSCC has six local maxima, nine saddles (3,-1), and five local minima. The corresponding atomic graph is shown in Figure 1e. It has six vertexes (three above and three below the second nearest neighbors) linked by twelve edges.

Despite the different kinds of graphs obtained for the metals, we conclude from Table 1 that the calculated values of $L(\mathbf{r})$ at the minima vary as a function of the d-band filling, f_d , and systematically increase as we move to the right along the first TM row of the Periodic Table. However, because ΔH_{ads} measures, to a certain extent, the capability that the adsorbed molecule has for forming a bond with the TM atom, and, in view of the fact that this bonding is related to the degree to which the d-band is unoccupied, we have plotted Figure 2, which is the value of $L(\mathbf{r})$ at the minima against $(1 - f_d)$ (where $f_d = N_d/10$ and N_d = the number of d electrons). It is interesting to note from this picture that the sequence has the same trend as that evinced by ΔH_{ads} .

In Figure 3, we have plotted the experimentally available^{14,23} heats of adsorption for the molecules O_2 and CO on polycrystalline TM surfaces as a function of the $L(\mathbf{r})$ values at the (3, +1) CP of the bulk atoms. We observe that there is a systematic decrease of ΔH_{ads} with the values of $L(\mathbf{r})$ at the local minima. This result implies that the bonds that O_2 and CO form with the TM become stronger as the value of $L(\mathbf{r})$ at the local minima of the VSCC decreases. This is a reasonable result when

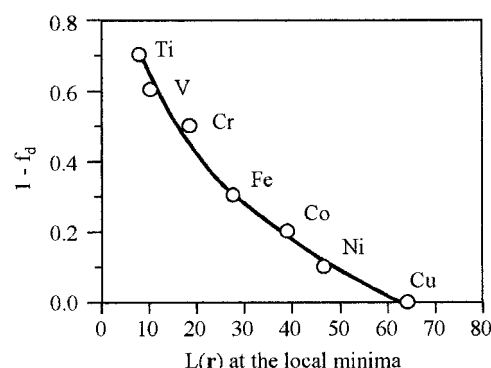


Figure 2. $L(\mathbf{r})$ value at the local minima of the metallic atom VSCC as a function of the d-band degree of nonoccupation ($1 - f_d$; $f_d = N_d/10$, N_d = the number of d electrons).

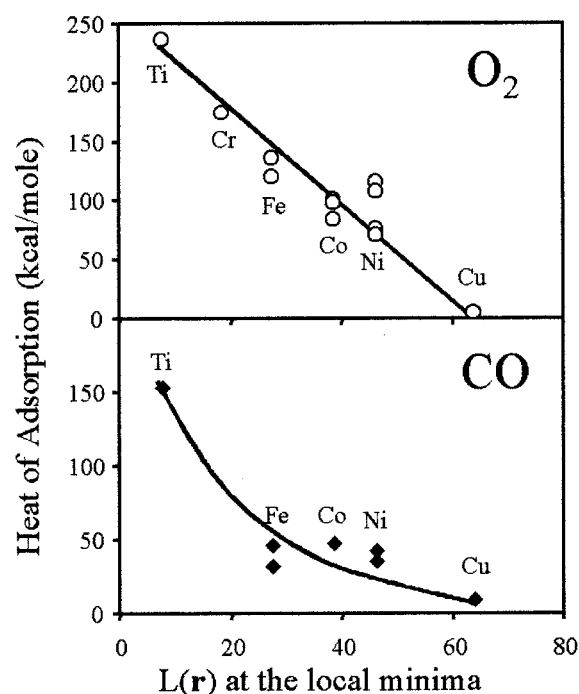
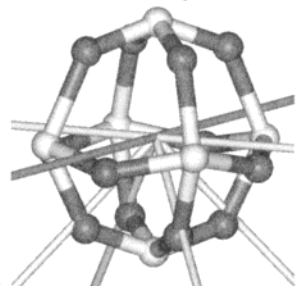
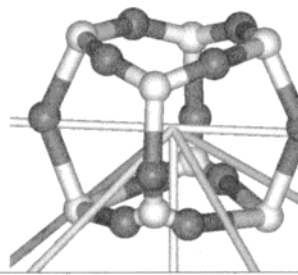
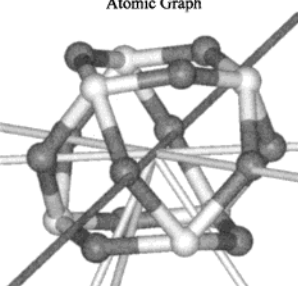
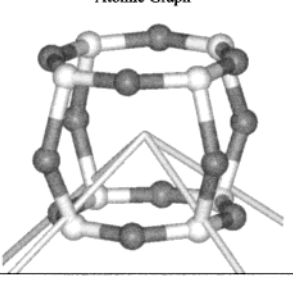
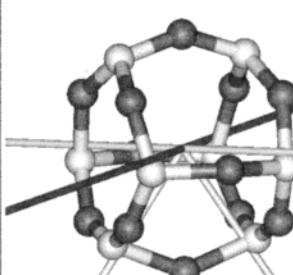
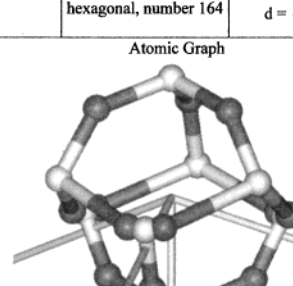


Figure 3. Experimental heat of adsorption (ref 14, 23) of O_2 and CO on polycrystalline surfaces of the 3d transition metals as a function of the $L(\mathbf{r})$ value at the local minima of the bulk atom VSCC.

we bear in mind that these local minima are a measure of the degree to which the d-band is unoccupied (and hence available to bond formation). Note, however, that several difficulties arise when trying to compare the Laplacian and the ΔH_{ads} values. An ab initio determination of the Laplacian has meaning at 0 K. On the other hand, the ΔH_{ads} are determined at room temperature. The ΔH_{ads} changes as the experimental conditions (temperature, adsorbate concentration, etc.) are varied. The adsorbate may modify its bonding as a result of temperature variations as well as of adsorbate concentration. Thus, in general, it is quite difficult to assign a single, definitive value to the heat of adsorption because surface preparation and cleanliness are not reproducible between different laboratories or even between batches of the same substrate material in the same laboratory. Thus, for example, the reported values of the ΔH_{ads} for oxygen adsorption on Ni (probably the most widely studied of the 3d TM) range from 70.0 to 120.0 kcal/mol. The values of ΔH_{ads} used in Figure 3 are those obtained for polycrystalline surfaces. Certainly, these surfaces may give rise to several different atomic graphs (the surface atoms have fewer neighbors

TABLE 2. Critical Points of L(r) in the Top Atoms VSCC of the Transition Metals Surfaces (au)

a	Surface	Cell ^d	Cell Parameters	Critical Points ^b	Ni ^c	Cu	
	100	P4/nmm, tetragonal, number 129	$\frac{\sqrt{2}}{2}a \times \frac{\sqrt{2}}{2}a \times 10d$ $d = a/2$	One (3,-3) above Four (3,-3) in One (3,-3) below Four (3,-1) above Four (3,-1) in Four (3,-1) below Four (3,+1) above Four (3,+1) below	57.750 0.551 55.340 0.552 56.754 0.551 49.479 0.556 50.444 0.555 50.423 0.555 47.759 0.557 48.664 0.556	66.874 0.529 68.814 0.528 67.290 0.528 65.113 0.529 65.952 0.529 64.389 0.529 63.787 0.530 64.380 0.529	
	Atomic Graph						
b	Surface	Cell	Cell Parameters	Critical Points	Ni		
	110	Pmmn, orthorhombic, number 59	$a \times \frac{\sqrt{2}}{2}a \times 12.5d$ $d = \frac{\sqrt{2}}{4}a$	Four (3,-3) above Four (3,-3) below Four (3,-1) above Four (3,-1) in Four (3,-1) below One (3,+1) above Four (3,+1) in One (3,+1) below	56.714 0.552 60.036 0.550 54.030 0.553 52.755 0.554 52.847 0.554 43.447 0.559 44.685 0.558 42.996 0.559		
	Atomic Graph						
c	Surface	Cell	Cell Parameters	Critical Points	Ni	Cu	
	111	P3m1, trigonal-hexagonal, number 164	$\frac{\sqrt{2}}{2}a \times \frac{\sqrt{2}}{2}a \times 8d$ $d = \frac{\sqrt{3}}{3}a$	Three (3,-3) above Three (3,-3) below Three (3,-1) above Six (3,-1) in Three (3,-1) below One (3,+1) above Three (3,+1) above Three (3,+1) below One (3,+1) below	57.332 0.551 59.022 0.550 51.583 0.554 48.200 0.556 52.281 0.554 46.484 0.557 46.818 0.557 47.467 0.556 42.963 0.559	66.820 0.528 68.218 0.528 65.340 0.529 65.582 0.529 65.608 0.529 65.257 0.529 64.393 0.529 65.161 0.529 64.019 0.530	
	Atomic Graph						
d	Surface	Cell	Cell Parameters	Critical Points	V	Cr	Fe
	100	P4/nmm, tetragonal, number 129	$a \times a \times 10d$ $d = a/2$	Four (3,-3) above Four (3,-3) below Four (3,-1) above Four (3,-1) in Four (3,-1) below One (3,+1) above Four (3,+1) in One (3,+1) below	12.270 0.727 12.952 0.725 12.750 0.725 11.859 0.728 12.093 0.727 11.095 0.730 11.319 0.729 10.696 0.731	19.404 0.679 18.801 0.680 18.907 0.680 16.224 0.685 18.257 0.681 13.525 0.690 14.630 0.688 13.286 0.691	31.653 0.612 31.014 0.612 31.482 0.612 29.083 0.614 30.815 0.612 26.336 0.617 28.509 0.615 27.519 0.616
	Atomic Graph						
e	Surface	Cell	Cell Parameters	Critical Points	Fe		
	110	Cmma, orthorhombic, number 67	$a \times \sqrt{2}a \times 10d$ $d = \frac{\sqrt{2}}{2}a$	Two (3,-3) above Four (3,-3) in Two (3,-3) below One (3,-1) above Four (3,-1) above Two (3,-1) in Four (3,-1) below One (3,-1) below Two (3,+1) above Two (3,+1) in Two (3,+1) below	33.322 0.610 33.646 0.610 32.417 0.611 30.989 0.612 31.848 0.611 29.929 0.613 32.249 0.611 28.084 0.615 26.037 0.617 25.182 0.618 26.715 0.616		
	Atomic Graph						
f	Surface	Cell	Cell Parameters	Critical Points	Fe		
	111	P3m1, trigonal-hexagonal, number 164	$\sqrt{2}a \times \sqrt{2}a \times 16d$ $d = \frac{\sqrt{3}}{6}a$	One (3,-3) above Three (3,-3) above Three (3,-3) below One (3,-3) below Three (3,-1) above Six (3,-1) in Three (3,-1) below Three (3,+1) above Three (3,+1) below	34.213 0.609 33.817 0.610 31.379 0.612 34.544 0.609 30.438 0.613 31.372 0.612 29.146 0.614 25.786 0.618 26.230 0.617		
	Atomic Graph						

^a Standard notation in Hahn, T. *International Tables for Crystallography*; Kluwer: Boston, 1996. ^b The positions of the CPs are given with respect to the top layer. ^c In each line, the first and second rows give the L(r) value (1 au = 1 e/a₀⁵) at the CP and the radial distance (1 au = 1 a₀) nucleus-CP, respectively.

than bulk atoms) as well as to different binding energies for the absorbed species. Sites containing low Miller index surfaces, such as (100), (111), and (110) (which are the most stable single-crystal surfaces), and irregularities, such as steps and kinks, are present. Polycrystalline samples yield an average heat of adsorption for these sites.

To examine further the relation suggested by Figure 3, we have studied in detail the AGs for the top atoms of low-index surfaces for some select cases, again using the WIEN 97 program. The surfaces were modeled using cells of five atom layers fixed at bulk-terminated {100}, {110}, or {111} positions. Vacuum layers thicker than 10 Å were used to ensure that there were no interactions between adjacent slabs. In Table 2, we

display some of the properties characterizing these cells, such as, the AG, the CP number, the CP position with respect to the top layer, the radial distances nucleus-CP, and the L(r) values at the CP for the top VSCC atoms. For bcc structures, the top atoms of the most close-packed (110) surface have six touching neighbors, four in the top layer and two in the second one. The top atoms in (100) surface have four touching neighbors located in the second layer, whereas in the most open (111) surface, they have three first neighbors in the second layer and one in the fourth layer. However, regardless of their coordination, the top-atoms AG for the three surfaces studied form a cube with eight vertexes linked by twelve edges. This graph exhibits a minimum of charge or (3,+1) CP above the (100) surface, a

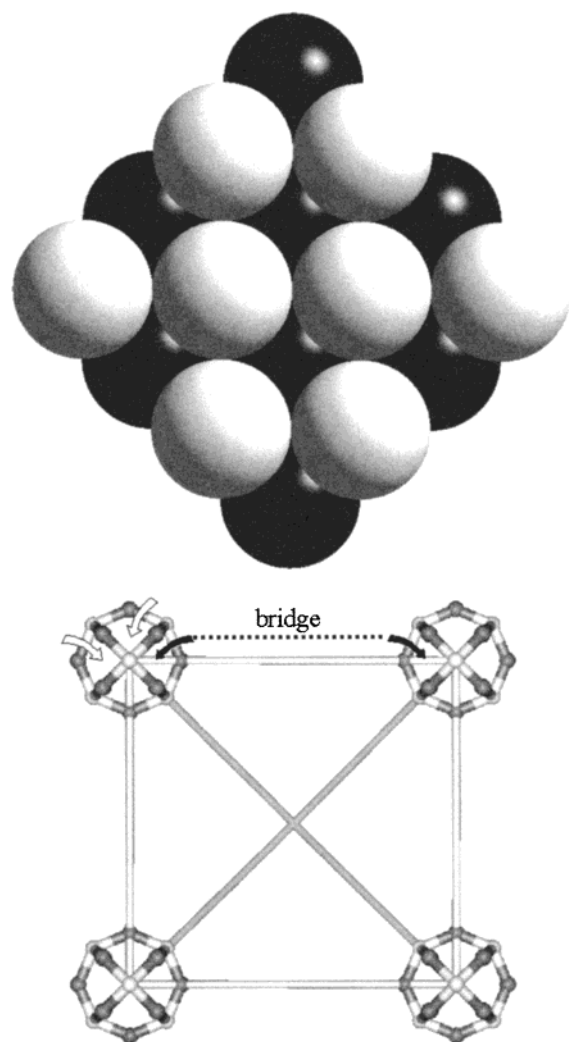


Figure 4. Top view of the (100) surface of fcc metals showing: (a) a ball model and (b) the atomic graph of the top atoms in the unit cell. In (a), white and black spheres denote the top and second layer atoms, respectively. Note that this surface only exposes the first and second layers. In (b), white and gray spheres denote the vertex and the edges of the graph, respectively. Long lines indicate bonds between closest atoms in the unit cell. The arrows point toward the local minima of the charge in the graph faces. White arrows show the attractive top site toward the local charge concentrations on the O_2 and CO molecule, whereas a pair of black arrows shows the corresponding bridge site.

local “peak” of charge surrounded by three (3,+1) CP above the (111) surface and a (3,-1) CP surrounded by two local charge concentrations and two local minima or (3,+1) CP above the (100) surface. For fcc structures, the top atoms of the most close-packed (111) surface have nine touching neighbors, six located in the first layer and three in the second. The top atoms of the (100) surface have eight touching neighbors, four located in the top layer and four located in the second layer, whereas in the most open (110) surface, there are six touching neighbors, two located in the top layer and four in the second. The AGs of the top atoms for the (100) and (111) surfaces, as was the case for fcc metals, are homeomorphic (they have the same number and kinds of critical points) with the bulk graph. This graph is an octahedron with six vertexes linked by twelve edges, and it exposes a (3,+1) CP surrounded by three (3,-3) CP above the (111) surface and a (3,-3) CP surrounded by four local minima above the (100) surface. The corresponding graph for the (110) surface is different from that of the fcc bulk and is homeomorphic to those of the bcc metals: a cube with eight vertexes linked

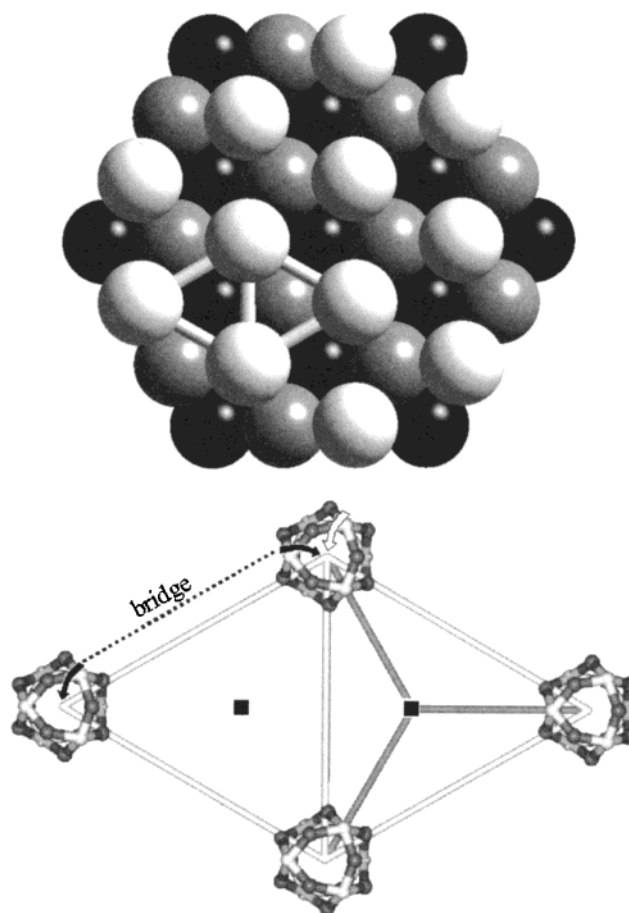


Figure 5. Top view of the (111) surface of fcc metals showing: (a) a ball model and (b) the atomic graph of the top atoms in the unit cell. In (a), white, gray, and black spheres denote the top, second, and third layer atoms, respectively. In (b), captions are similar to Figure 4b. A black square denotes the 3-fold sites in the (111) surface. Note that there are two types of 3-fold sites on this surface.

by twelve edges. This graph exhibits a (3,+1) CP, surrounded by four (3,-3) CP, outside the surface.

From these results, it is clear that the AGs on the different surfaces can exhibit very different environments to the incoming molecules. Laplacian topology predicts that the adsorption pathway is initially determined by the mutual alignment of the (3,-3) CP in the incoming molecule with the (3,+1) CP on the top atoms of the surfaces. CO adsorption,^{12,13} for example, involves attractive interaction between a vertex (a local charge concentration) on the C atom, C_V , with the (3,+1) CPs on the top atoms of the surface, F_{top} . In fcc metals, CO can adsorb on the (100) surface at the top and bridge sites (See Figure 4). Top-site adsorption involves the attractive interaction $C_V - F_{top}$ and bridge-site adsorption, that with two surface atoms: $F_{top} - C_V - F_{top}$. These results are in accord with experimental and theoretical findings:¹³ CO prefers to adsorb on the top site of the Cu and Ni (100) surfaces, but the adsorption energy difference between top-site and bridge-site adsorption is small and temperature-dependent. On the (111) surface, in addition to the top and bridge sites, CO can adsorb in a 3-fold position (See Figure 5) involving attractive interactions of the vertex on the C atom with faces located on the three top surface atoms. Theoretical calculations²⁴ of the CO heat adsorption on the Ni (111) surface have shown that the most stable adsorption site on this surface is the 3-fold one. But, as was the case with the (100) surface, the adsorption energy difference with respect to the other sites is small. The measured ΔH_{ads} should yield the

average of the heat of adsorption on those sites. The experimental ΔH_{ads} for the (100), (110), and (111) Ni surfaces are 30.0, 30.0, and 26.5 kcal/mol, respectively, whereas for the (100) and (111) Cu surfaces, they are 13.5 and 13.0 kcal/mol, respectively. This small change in the heat of adsorption for the different surfaces of the same metal agrees with predictions based on topological considerations. Thus, topology-based theory predicts that the attractive $C_V - F_{\text{top}}$ interactions will be stronger as the value of the Laplacian at the (3,+1) CP decreases. Nevertheless, as is shown in Table 2, these latter values remain quite similar for the different surfaces of a given metal. Note that for each one of these metals, regardless of the surface, the magnitude of the VSCC radius and the $L(r)$ value at the CP are very similar to those of the corresponding CP for the bulk. This is at the basis of the relationship shown in Figure 3. The strength of the bond formed in the process of adsorption depends on the chemical nature of the metallic atoms involved; this chemical nature is essentially characterized by the VSCC parameters, and they remain largely unchanged from the bulk to the surfaces.

Acknowledgment. The authors would like to thank CONICIT of Venezuela (Project No. S1-95001616) for providing funding for the SGI Origin 2000 and SGI O2 workstations used in this work. We also thank Professor Eduardo Ludeña for his careful reading of the manuscript and for his comments.

References and Notes

- (1) (a) MacDougall, P. J. The Laplacian of the Electronic Charge Distribution. Ph.D. Thesis, Department of Chemistry, McMaster University, Hamilton, Ontario, Canada, 1989. (b) MacDougall, P. J.; Hall, M. B. *Trans. Am. Crystallogr. Assoc.* **1990**, 26, 105. (c) Bader, R. F. W.; Essén, H. *J. Chem. Phys.* **1984**, 80, 1943. (d) Shi, Z.; Boyd, R. J. *J. Chem. Phys.* **1988**, 88, 4375.
- (2) Bader, R. F. W.; MacDougall, P. J.; Lau, C. D. H. *J. Am. Chem. Soc.* **1984**, 106, 1594.
- (3) Bader, R. F. W.; MacDougall, P. J. *J. Am. Chem. Soc.* **1985**, 107, 6788.
- (4) Bader, R. F. W.; Popelier, P. L. A.; Chang, C. J. *Mol. Struct.* Bader, R. F. W.; Popelier, P. L. A.; Chang, C. J. *THEOCHEM* **1992**, 255, 145.
- (5) Bader, R. F. W. *Atoms in Molecules—a Quantum Theory*; Clarendon Press: Oxford, U. K., 1990.
- (6) Carrol, M. T.; Chang C.; Bader, R. F. W. *Mol. Phys.* **1988**, 63, 387.
- (7) Tsirelson, V. G.; Zou, P. F.; Tang, T.-H.; Bader, R. F. W. *Acta Crystallogr.* **1995**, A51, 143.
- (8) Aray, Y.; Bader, R. F. W. *Surf. Sci.* **1996**, 351, 233.
- (9) Aray, Y.; Rosillo, F.; Murgich, J. *J. Am. Chem. Soc.* **1994**, 116, 10 639.
- (10) Aray, Y.; Rodriguez, J.; Murgich, J.; Ruetter, F. *J. Phys. Chem.* **1993**, 97, 8393.
- (11) Aray, Y.; Rodriguez, J. *Can. J. Chem.* **1996**, 74, 1014.
- (12) Aray, Y.; Rodriguez, J. *Surf. Sci.* **1998**, 405, L532.
- (13) Aray, Y.; Rodriguez, J.; Rivero, J.; Vega, D. *Surf. Sci.* **1999**, 441, 344.
- (14) Somorjai, G. A. *Introduction to Surface Chemistry and Catalysis*; John Wiley & Sons: New York, 1994.
- (15) Norskov, J. K. *Rep. Prog. Phys.* **1990**, 53, 1253.
- (16) Van Santen, R. A. *Rec. J. R. Neth. Chem. Soc.* **1982**, 101, 121.
- (17) Whitten, J. L.; Yang, H. *Surf. Sci. Rep.* **1996**, 24, 55.
- (18) Blaha, P.; Schwarz, K.; Luitz, J. *WIEN 97*, Vienna University of Technology 1997. (Improved and updated Unix version of the original copyrighted WIEN-code, which was published by Blaha, P.; Schwarz, K.; Sorantin, P.; Trickey, S. B. *Comput. Phys. Commun.* **1990**, 59, 399).
- (19) Perdew, J. P.; Burke, S.; Ernzerhof, M. *Phys. Rev. Lett.* **1996**, 77, 3865.
- (20) Bader, R. F. W.; Krugg, P. Department of Chemistry. McMaster University, Hamilton, Ontario, Canada. 1990.
- (21) Aray, Y.; Rodriguez, J.; López-Boada, R. *J. Phys. Chem.* **1997**, 101, 2178.
- (22) Barret, C. S.; Massalski, T. B. *Structure of Metals*; McGraw-Hill, USA. 1966.
- (23) Toyoshima, I.; Somorjai, G. A. *Catal. Rev.—Sci. Eng.* **1979**, 19, 105.
- (24) Van Langelveld, A. D.; De Koster, A.; Van Santen, R. A. *Surf. Sci.* **1990**, 225, 143.